JACS
JOURNAL OF THE AMERICAN CHEMICAL SOCIETY
pubs.acs.org/JACS
Article

Two-Dimensional Peptide Assembly *via* Arene−Perfluoroarene Interactions for Proliferation and Differentiation of Myoblasts

Taeyeon Kim, Jinwoo Hong, Jehan Kim, Jinhan Cho, and Yongju Kim*

Cite This: *J. Am. Chem. Soc.* 2023, 145, 1793−1802
Read Online
ACCESS | Metrics & More | Article Recommendations | Supporting Information

ABSTRACT: Supramolecular assembly based on aromatic interactions can provide well-defined nanostructures with an understanding of intermolecular interactions at the molecular level. The peptide assembly *via* a supramolecular approach can overcome the inherent limitations of bioactive peptides, such as proteolytic degradations and rapid internalizations into the cytosol. Although extensive research has been carried out on supramolecular peptide materials with a two-dimensional (2D) structure, more needs to be reported on biological activity studies using well-defined 2D peptide materials. Physical and chemical properties of the 2D peptide assembly attributed to their large surface area and flexibility can show low cytotoxicity, enhanced molecular loading, and higher bioconjugation efficiency in biological applications. Here, we report supramolecular 2D materials based on the pyrene-grafted amphiphilic peptide, which contains a peptide sequence (Asp-Gly-Glu-Ala; DGEA) that is reported to bind to the integrin $\alpha 2\beta 1$ receptor in 2D cell membranes. The addition of octafluoronaphthalene (OFN) to the pyrene-grafted peptide could induce a well-ordered 2D assembly by face-centered arene−perfluoroarene stacking. The DGEA-peptide 2D assembly with a flat structure, structural stability against enzymatic degradations, and a larger size can enhance the proliferation and differentiation of muscle cells *via* continuous interactions with cell membrane receptors integrin $\alpha 2\beta 1$ showing a low intracellular uptake (15%) compared to that (62%) of the vesicular peptide assembly. These supramolecular approaches *via* the arene−perfluoroarene interaction provide a strategy to fabricate well-defined 2D peptide materials with an understanding of assembly at the molecular level for the next-generation peptide materials.

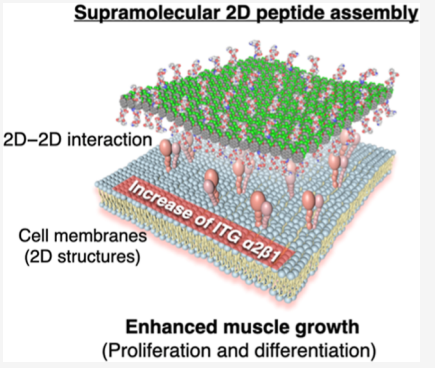

INTRODUCTION

Supramolecular assembly based on non-covalent intermolecular interactions is an attractive tool for the sophisticated fabrication of various nanostructures.[1] Among various self-assembling building blocks, aromatic amphiphiles, consisting of hydrophobic aromatic segments and hydrophilic flexible segments, are good candidates for well-defined supramolecular structures with a hydrophobic aromatic core surrounded by hydrophilic flexible segments in an aqueous solution.[2] The well-defined supramolecular materials conjugated with biomolecules have been reported for many biological applications such as molecular deliveries,[3] bio-imagings,[4] and multivalent bioactive ligands.[5] An understanding of the intermolecular aromatic interactions at the molecular level can provide considerable insights into the control strategy of the size, dimension, and property of the desired supramolecular materials.

Peptides derived from proteins can become important in the selective regulation of biological systems such as cell adhesions,[6] proliferations,[7] and differentiations.[8] Nonetheless, many short linear peptides have limitations in achieving sufficient bioactivity due to proteolytic degradations and rapid internalizations into the cytosol without sufficient stimulation of membrane surface receptors.[9] Recent developments in peptide-based materials using a supramolecular approach have led to improvements in peptide properties and their bioactivity to overcome conventional limitations.[10] Supramolecular nanofibers,[11] micelles,[12] and vesicles[13] with bioactive peptides have been reported to regulate the target receptors by mimicking native ligand proteins. Although extensive research has been carried out on supramolecular peptide materials with a two-dimensional (2D) structure,[14] more needs to be reported on biological activity studies using well-defined 2D materials by self-assembly of peptides. 2D peptide assembly can provide a novel perspective in the development of functional materials for biological applications due to the physical and chemical properties of 2D structures, attributed to their large surface area and flexibility, showing low cytotoxicity, enhanced molecular loading, and higher bioconjugation efficiency.[15]

Here, we report the formation of supramolecular vesicles and 2D materials *via* self-assembly of the pyrene-grafted amphiphilic peptide, **2**, which contains a peptide sequence (Asp-Gly-Glu-Ala; DGEA) derived from collagen type I proteins as a typical

Received: October 15, 2022
Published: January 10, 2023

https://doi.org/10.1021/jacs.2c10938
J. Am. Chem. Soc. 2023, 145, 1793−1802

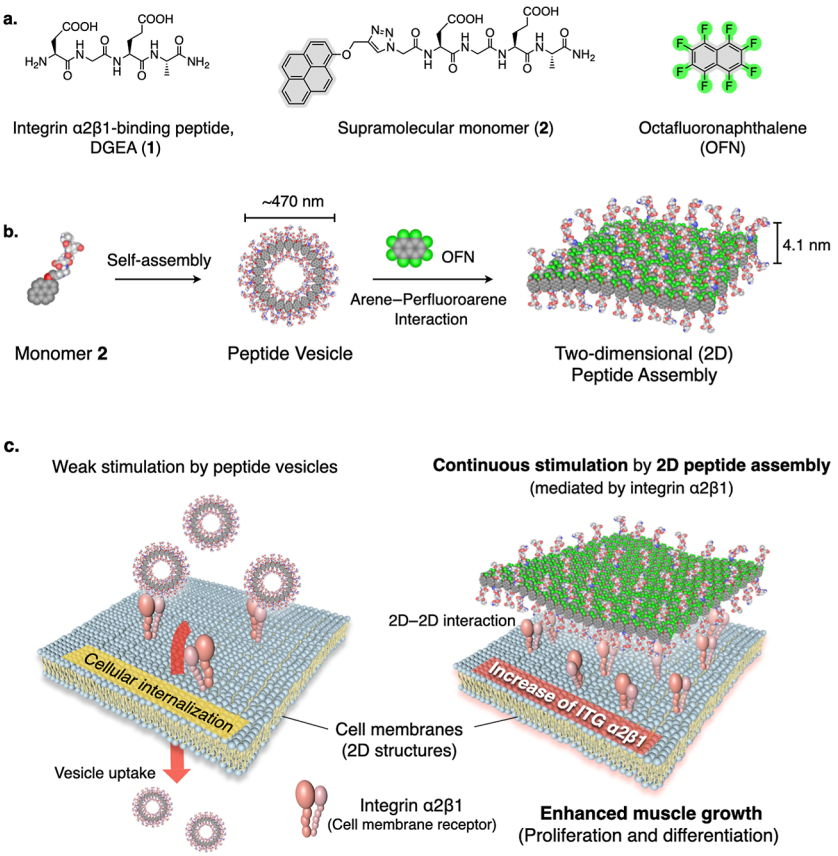

Figure 1. 2D peptide assembly *via* arene–perfluoroarene interactions and their activities on proliferation and differentiation of the myoblast. (a) Chemical structures of peptide **1**, peptide **2**, and OFN. (b) Formation of a vesicle and 2D sheet structure triggered by the addition of OFN *via* arene–perfluoroarene interactions. (c) Representation of the different biological activities of the vesicles and sheet for regulations of proliferation and differentiation of myoblasts.

Scheme 1. Synthetic Method of Peptide 1 and Peptide 2[a]

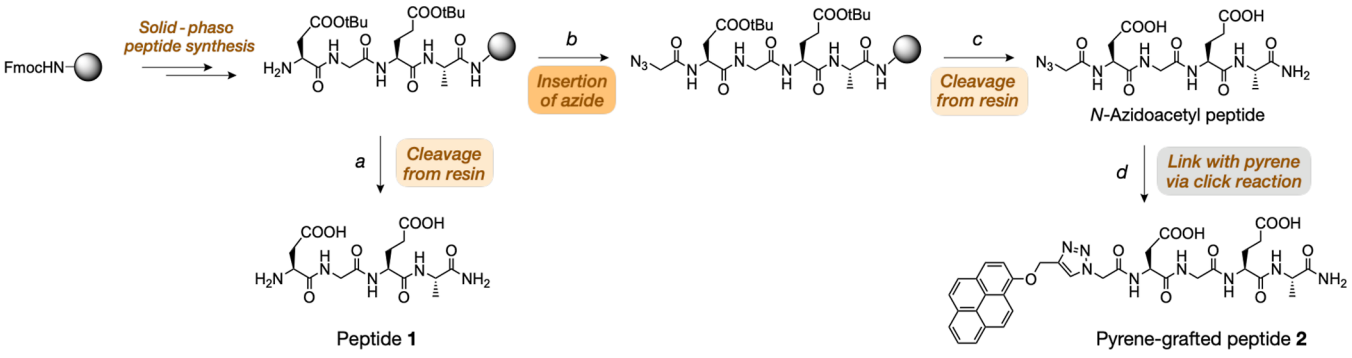

[a]Reagents and condition: (a) TFA: anisole: water = 90: 5: 5 (*v*/*v*), room temperature (rt), 2 h, 15%; (b) azidoacetic acid, HCTU, DIPEA, DMF, rt, 2 h; (c) TFA/anisole/water = 90:5:5 (*v*/*v*), rt, 2 h, 14.8%; and (d) *N*-azidoacetyl peptide, 1-(prop-2-yn-1-yloxy)pyrene, sodium ascorbate, $CuSO_4$, H_2O/EtOH (1:3, *v*/*v*), rt, 16 h, 89%; Abbreviations: trifluoroacetic acid: TFA, *O*-(1*H*-6-chlorobenzotriazol-1-yl)-1,1,3,3-tetramethyluronium hexafluorophosphate: HCTU, *N*,*N*-diisopropylethylamine: DIPEA, *N*,*N*-dimethylformamide: DMF, ethanol: EtOH, and copper(II) sulfate: $CuSO_4$.

natural extracellular matrix that is reported to bind to the integrin $\alpha 2\beta 1$ receptor in 2D cell membranes.[16] The amphiphilic peptide **2** self-assembles into vesicles with a size of approximately 470 nm in an aqueous solution *via* aromatic interactions (Figure 1b). The addition of octafluoronaphthalene (OFN) to the pyrene-grafted peptide could induce a well-ordered 2D assembly with a size of several micrometers by face-centered arene–perfluoroarene stackings.[18] DGEA-coated 2D materials with a flat structure, structural stability against enzymatic degradations, and a larger size can enhance the proliferation and differentiation of muscle cells, C2C12, *via* continuous interactions with cell membrane receptors integrin $\alpha 2\beta 1$ showing a low intracellular uptake (15%) compared to that (62%) of the vesicular peptide assembly (Figure 1c). These results provide a strategy to fabricate peptide-based 2D materials *via* a supramolecular approach with an understanding of assembly at the molecular level for the improved biological activity of peptides.

https://doi.org/10.1021/jacs.2c10938
J. Am. Chem. Soc. 2023, 145, 1793−1802

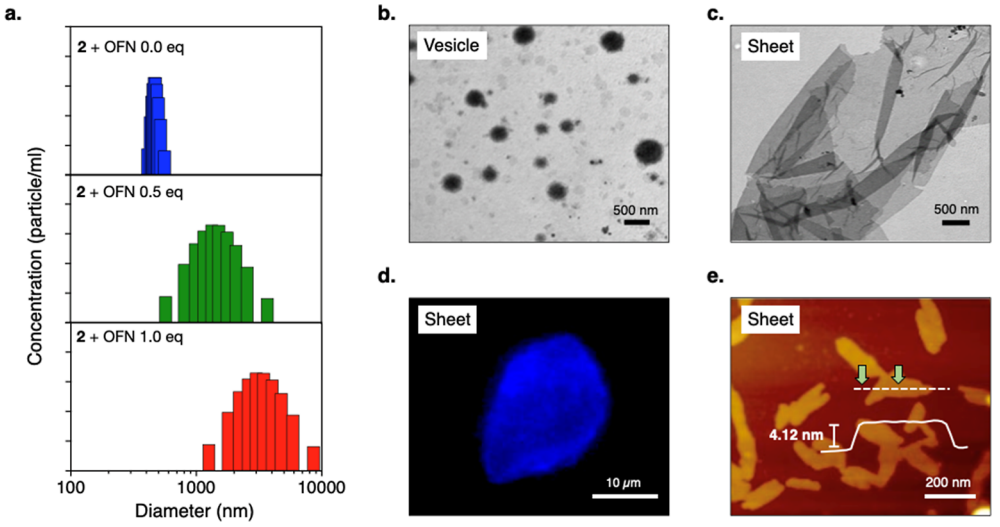

Figure 2. Structural characterizations of the 2D peptide assembly. (a) Size distributions from DLS measurements of peptide **2** (137 μM) solutions with different equivalents of OFN. (b,c) Negatively stained TEM images of peptide **2** (vesicles, 275 μM) and peptide **2** with 1 equivalent of OFN (sheets, 275 μM) in a pH 7.4 phosphate buffer. (d) FOM image of peptide **2** (1.37 mM) solution with OFN (1.37 mM) in a pH 7.4 phosphate buffer. Excitation filter at λ_{ex} = 340−380 nm. (e) AFM height image of 2D sheets on a mica film. The cross-sectional profile (middle) is taken along the white dotted line.

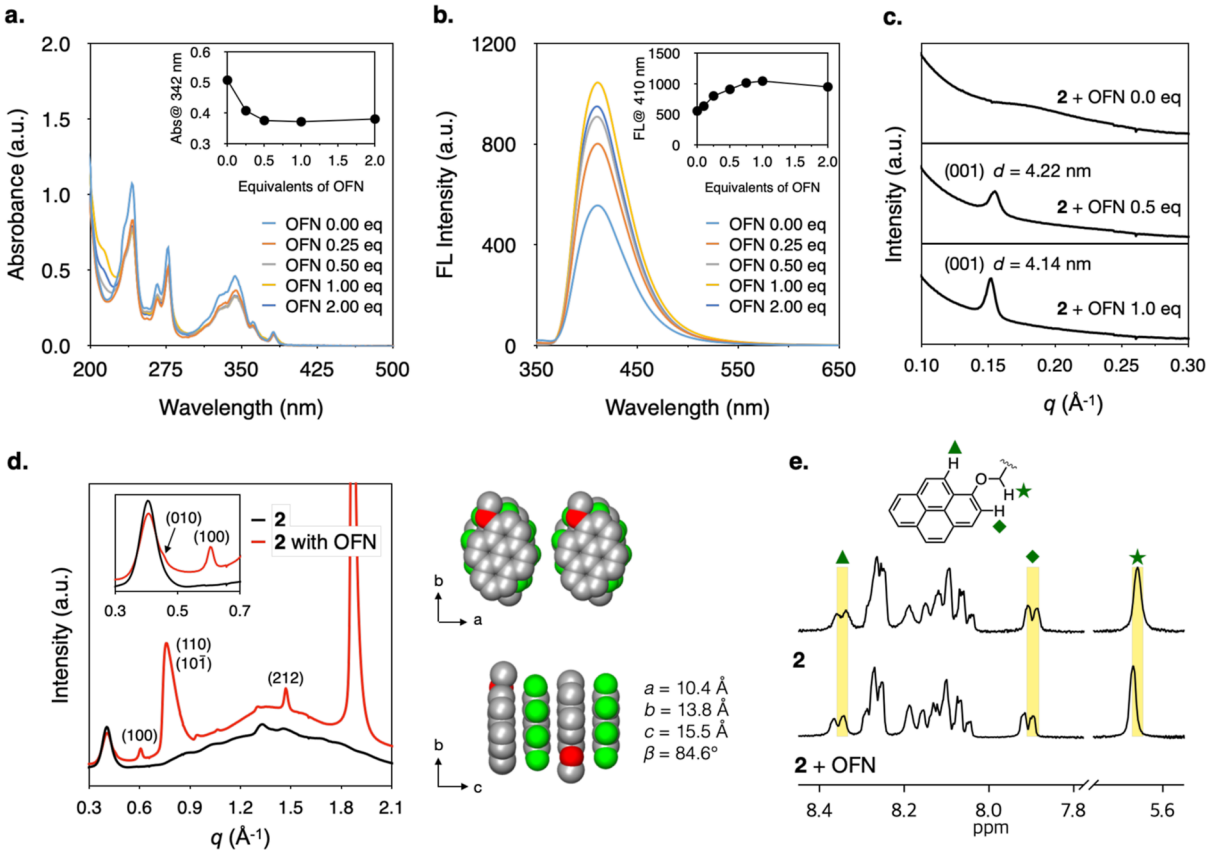

Figure 3. Spectroscopic analysis for the 2D peptide assembly obtained *via* arene−perfluoroarene interactions. (a) Absorption spectra of peptide **2** (687 μM) with different equivalents of OFN in a pH 7.4 phosphate buffer. (b) Emission spectra (excitation wavelength, 342 nm) of peptide **2** (687 μM) with different equivalents of OFN. (c) SAXS patterns of dried samples of peptide **2** with different equivalents of OFN. (d) WAXS patterns of dried samples of peptide **2** with and without 1 equivalent of OFN. The molecular packing mode in a 3D monoclinic structure with lattice parameters is shown. (e) ^{1}H NMR spectra of peptide **2** (687 μM) with and without OFN (687 μM) in D_2O buffered with phosphate.

RESULTS AND DISCUSSION

The DGEA peptide sequence is highly soluble in aqueous solutions due to the inherent negatively charged residues of Asp and Glu. To endow the peptide chain with self-assembling features, a hydrophobic aromatic pyrene was grafted into the hydrophilic DGEA because the self-assembly of aromatic amphiphiles can provide well-defined supramolecular structures *via* the preferred associations of rigid aromatic segments such as

https://doi.org/10.1021/jacs.2c10938
J. Am. Chem. Soc. 2023, 145, 1793−1802

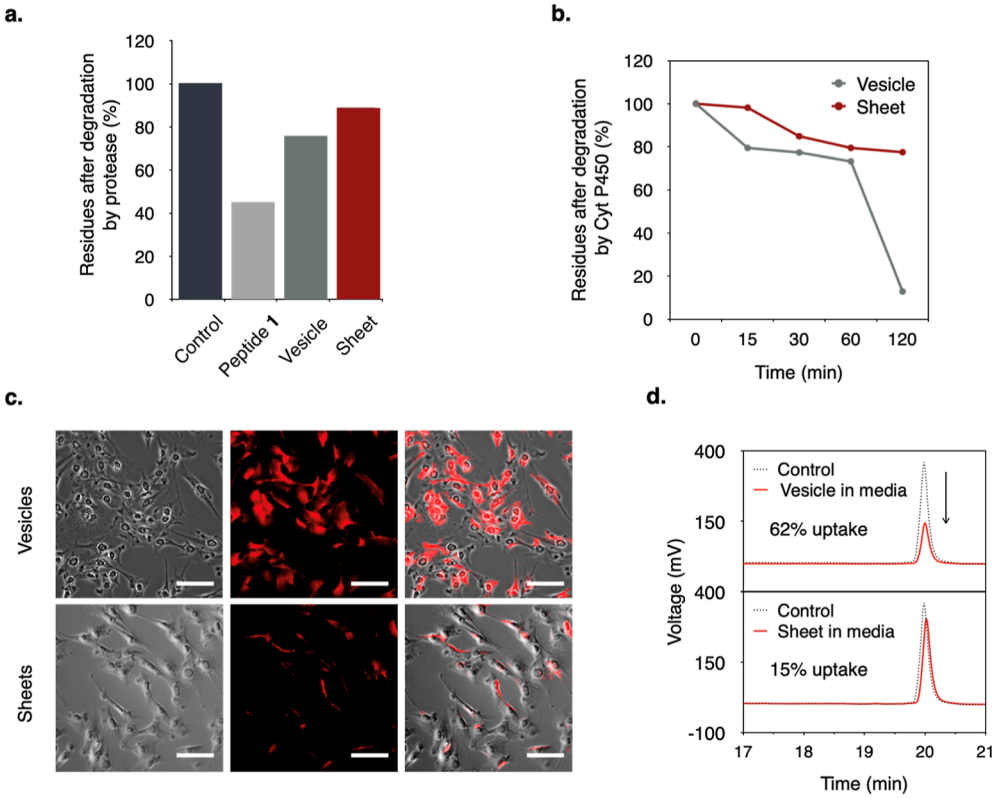

Figure 4. Structural stability against enzymatic degradations and uptake resistance of the vesicles and sheets as peptide assemblies. (a) Residues after degradation of peptide **1**, supramolecular vesicles (peptide **2**), and sheets (peptide **2** with 1 equivalent of OFN) by protease from the bovine pancreas. The residual quantities of peptide **1** and **2** were calculated from the HPLC peak area measurements. Control means no treatment with protease. (b) HPLC analysis for the degradation rate of supramolecular vesicles and sheets by the Cyt P450 oxidative enzyme. Peptide **2** residues were calculated from the HPLC peak area measurements. (c) FOM images of C2C12 cells treated by vesicles or sheets (excitation filter at λ_{ex} = 530−560 nm). The images were obtained after 4 h of incubation with vesicles or sheets. Scale bar, 50 μm. (d) HPLC analysis of the residual quantity of peptide **2** for vesicles and sheets in the cell culture media. Control means peptide **2** in the media without cells.

an either edge-to-face or face-to-face orientation.[19] As the first step, an *N*-azidoacetyl DGEA peptide building block was synthesized using a solid-phase peptide synthesis method (Scheme 1 and Figure S1). The *N*-terminal azido group of the resulting peptide was reacted with an acetylene-attached pyrene *via* click chemistry to obtain the target amphiphilic peptide **2** (Scheme 1 and Figures S2 and S3).

To investigate the structures of the self-assembled amphiphilic peptide **2** in an aqueous solution, we performed dynamic light scattering (DLS) measurements and transmission electron microscopy (TEM) experiments.

DLS study showed that the aggregate size was ∼470 nm (Figure 2a), and the negatively stained TEM image of peptide **2** showed a vesicle shape with an average size of 495 nm (Figures 2b, S4, and S5). Considering the size of a few tens of micrometers of native proteins[17] in extracellular environments, which interact with membrane receptors, the design of self-assembled objects with a size of several micrometers is required. To increase the dimension of the materials, hydrophobic aromatic guests were added to induce well-ordered aromatic interactions. Among several aromatic interactions, arene−perfluoroarene interactions were chosen due to the abiotic nature of perfluoroarenes, providing bioorthogonal noncovalent interactions.[18] Several perfluorinated aromatic molecules [such as OFN, tetra-1,4-benzoquinone (fluoranil), and hexafluorobenzene (HFB)] (as electron-poor aromatic guests) were added to induce arene−perfluoroarene interactions with the pyrene group of peptide **2** as an electron-rich aromatic segment. DLS experiments showed the gradually increased size of aggregates in the presence of 0.5 and 1.0 equivalents of OFN (Figure 2a). The absorbance at 342 nm sequentially decreased (Figure 3a), and the fluorescence intensity at 410 nm increased up to 1.0 equivalent of OFN (Figure 3b); with the further addition of OFN, absorbance and fluorescence intensity did not change significantly.

Negatively stained TEM and fluorescence optical microscopy (FOM) images showed that peptide **2** with 1.0 equiv of OFN could form well-defined supramolecular 2D sheets with a size of a few tens of micrometers (Figure 2c,d and S6−S8). In contrast to the OFN complex, a complex of peptide **2** with fluoranil or HFB showed irregular aggregates, indicating that fluoranil or HFB could not form significant arene−perfluoroarene interactions with the pyrene group (Figures S9 and S10). Therefore, an equal ratio of peptide **2** and OFN (1:1) was selected as an optimal condition for further experiments.

To obtain further information on the mechanism for the sheet formation, a pristine solution without sufficient aging time after sonication of peptide **2** with 1 equiv of OFN in a pH 7.4 phosphate buffer was subjected to TEM measurement. The TEM image indicated 2D sheet structures with in-plane, parallel arrangement of the primary nanofibers, demonstrating that the preformed nanofibers were laterally associated to generate the planar sheet structures (Figure S11). Atomic force microscopy (AFM) measurement of the 2D materials obtained by drop-casting of the aqueous solution on a mica surface revealed that the sheets were very flat with a uniform thickness of 4.1 nm

https://doi.org/10.1021/jacs.2c10938
J. Am. Chem. Soc. 2023, 145, 1793−1802

(Figure 2e). This result indicates that the pyrenes of **2** and OFN are arranged in a monolayer with the peptide surfaces, in which the aromatic segments are aligned parallel to the sheet plane, and hydrophilic DGEA-peptide chains are exposed to the aqueous environment. X-ray diffraction (XRD) measurements were performed to understand the molecular arrangements within the 2D sheets. The small-angle X-ray scattering (SAXS) diffraction patterns revealed a reflection of 4.14 nm at the *d*-spacing between sheets, which was close to the thickness obtained from the AFM result (Figures 3c and S12). Wide-angle X-ray scatterings (WAXS) showed several sharp reflections that agree well with the expected relative peak positions for a 3D monoclinic structure with lattice parameters of a = 10.41 Å, b = 13.78 Å, c = 15.45 Å, and β = 84.57° (Figures 3d and S13). A strong reflection at 3.37 Å associated with the $\pi-\pi$ stacking distance indicated the close parallel packing of aromatic segments (Figure S14b). In contrast, WAXS results of peptide **2** without OFN and OFN alone revealed only a broad and weak reflection in similar q-values, indicative of a lack of crystallinity (Figures 3d and S15). The associations between pyrene and OFN in the solution state were also confirmed *via* proton nuclear magnetic resonance (^{1}H NMR) experiments in deuterium oxide (D_2O). The ^{1}H NMR resonances associated with the aromatic protons and OCH_2 of peptide **2** were shifted downfield in the presence of OFN, and the change in the chemical shift was consistent with a face-centered stacking interaction between pyrene and OFN (Figure 3e). Furthermore, we performed 2D nuclear Overhauser effect (NOE) NMR experiments of peptide **2** (vesicles) and peptide **2** with OFN (sheets) in D_2O (Figures S16 and S17). The NOE correlation intensity in the pyrene group (there are two kinds of correlations, such as intramolecular and intermolecular correlations) decreased in peptide **2** with OFN compared with that in peptide **2**, indicating that the distance between the pyrenes increased due to the specific interaction of pyrene−OFN. Computational molecular simulations based on density functional theory (DFT) revealed that the association between pyrene and OFN was a molecularly opposite arene−perfluoroarene interaction between pyrene carbons with a partial negative charge and OFN carbons with a partial positive charge, which could induce a strong aromatic interaction *via* electrostatic attractions[18] (Figures S14a and S18). Cumulatively, the data suggest that the supramolecular assembly of peptide **2** and OFN *via* arene−perfluoroarene interactions can be described as a well-defined flat 2D assembly, showing the exposed DGEA peptides on the sheet surfaces.

The stability of peptide **2** in the 2D peptide assembly was measured by enzymatic degradation experiments based on protease and cytochrome P450 1A2 (CYP1A2). High-performance liquid chromatography (HPLC) analysis revealed that 55% of peptide **1**, 24% of peptide **2** in vesicles, and 11% of peptide **2** in sheets were degraded by mixing with protease from the bovine pancreas for 15 min (Figures 4a and S19). The higher stability of peptide **2** in the sheets was also observed *via* a slower degradation rate than that in the vesicles by CYP1A2, which can metabolize polycyclic aromatic hydrocarbons[20] (Figure 4b). These results implied that both the exposed peptide segment and the inner aromatic core showed higher stability against enzymatic degradations in the 2D peptide assembly due to the compact molecular packing in a large 2D structure *via* the arene−perfluoroarene interaction triggered by the addition of OFN. Considering the large size, flat structure, and structural stability of sheets attributed to $\pi-\pi$ stacking and lateral hydrophobic interaction in the co-assembly of peptide **2** and OFN, resistance to the cellular uptake of sheets was demonstrated *via* FOM and HPLC analysis. The FOM images showed the spreading of vesicles into the cells after 4 h of incubation of the myoblasts (C2C12 cells).

In contrast, the sheets showed a lower degree of internalization into the cell, and the fluorescence of the sheets was observed predominantly on the cell surface in the FOM image (Figure 4c). The cellular uptake efficiency of vesicles and sheets was also studied by measuring the residual amount of peptide **2** in cell culture media *via* HPLC analysis after 4 day incubation (Figure 4d and Table 1). The HPLC peak intensity in the vesicles was significantly lower than that of the control in the media; this is indicative of a high intracellular uptake (62% uptake). In contrast, the sheets showed a little decrease in the HPLC peak intensity (15% uptake). Therefore, the 2D peptide assembly with relatively larger sizes, flat structures, and enhanced peptide stability would maintain the structure for the related functions in the extracellular environment with lower cellular internalization than those of the pure peptide and vesicle.

Table 1. HPLC Gradient Condition of the Mobile Phase

	percentage of the solvent (%)		
time (min)	H_2O	CH_3CN	flow rate (mL/min)
0	80	20	1
30	0	100	1

Monomeric DGEA peptide **1** and DGEA-based peptide assemblies such as vesicles (**2**) and sheets (**2** with OFN) were studied for the proliferation of C2C12 cells because the DGEA motif derived from collagen type I proteins can regulate cellular functions such as adhesion, proliferation, and differentiation by interacting with integrin $\alpha2\beta1$.[21] A methylthiazolyldiphenyltetrazolium bromide (MTT) assay was performed to measure cell proliferation and toxicity of the peptide assemblies. The materials showed biocompatibility without significant toxicity up to a concentration of 40 μM. Interestingly, only sheets could increase the proliferation rate of cells in contrast with peptide **1** and vesicles (Figure 5a). TEM and FOM measurements revealed that the sheet structures were maintained during dilution to 5, 20, and 40 μM concentrations in the cell culture media for biological studies (Figure S20). A 5 μM concentration was used in further experiments as it was associated with the most enhanced proliferation rate. In addition, the MTT assay using amorphous structures *via* peptide **2**−HFB and peptide **2**−fluoranil as control experiments showed little effect on cell proliferation, indicative of the importance of the 2D peptide structure (Figure S21). Zeta potential measurements showed negatively charged vesicles and sheets in the cell culture media due to the aspartate and glutamate side chains (Figure S22). To investigate the effect of peptide density in the sheets, an additional amphiphile molecule (**S1**) was synthesized by linking pyrene and oligoethylene glycol (Figure S23). Co-assembly of the three components was conducted in different molar ratios (peptide **2**/amphiphile **S1**/OFN: 100/0/100, 75/25/100, 50/50/100, 25/75/100, and 0/100/100). TEM images of all samples at the 5 μM concentration showed the 2D structures in an aqueous solution, indicating that the DGEA peptide density would be controlled sequentially in the materials. The MTT assay showed lower proliferation efficiency upon decreasing the

https://doi.org/10.1021/jacs.2c10938
J. Am. Chem. Soc. 2023, 145, 1793−1802

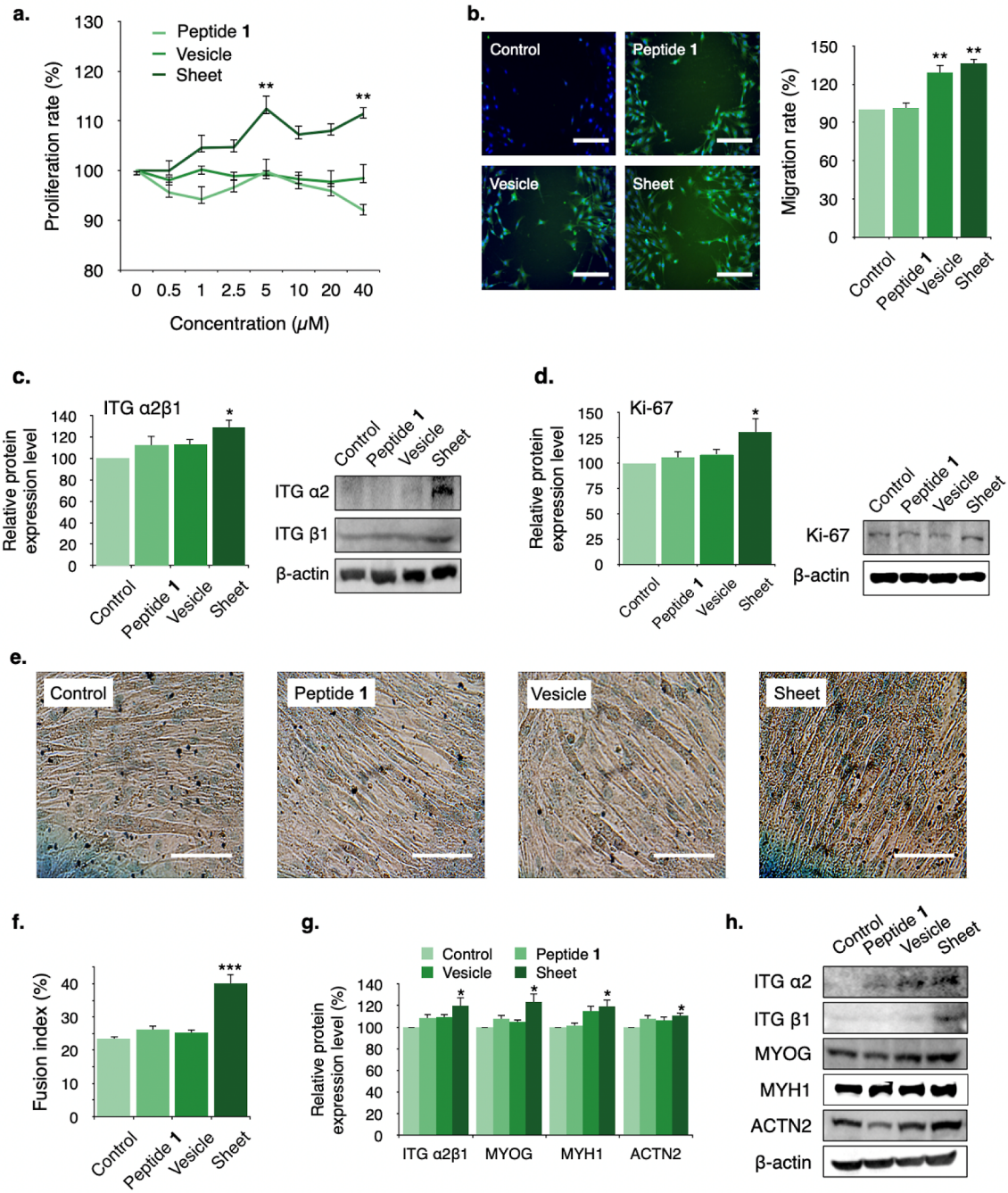

Figure 5. Proliferation and differentiation effects of C2C12 cells by the treatment of the peptide assemblies. (a) MTT assay of the concentration-dependent manner with peptide **1**, vesicles (peptide **2**), and sheets (peptide **2** with 1 equivalent of OFN) for proliferation and cell viability. (b) Wound healing assay after the treatment of peptide **1**, vesicles, and sheets, respectively. Merged fluorescence microscopy images obtained using an excitation filter at λ_{ex} = 340−380 nm and λ_{ex} = 450−490 nm. Scale bar, 200 μm. The levels of wound healing in the graph were calculated relatively from the ratio of the closure area to the area of the initial wound (0 h). (c,d) Protein expression levels of ITG $\alpha 2\beta 1$ and Ki-67 by fluorescence intensity *via* an ICC assay and western blots after the treatment of peptide **1**, vesicles, and sheets. The fluorescence intensity was measured using a microplate reader and is represented as a graph (excitation wavelength at λ_{ex} = 488 nm and emission wavelength at λ_{em} = 525 nm). (e) Representative Giemsa staining images at 4 days during muscle differentiation after the treatment of the peptide **1**, vesicles, and sheets. Scale bar, 100 μm. (f) Measurements of the fusion index for evaluations of myotube formation. (g) Fluorescence intensity graph (below) for the protein expression of ITG $\alpha 2\beta 1$, MYOG, MYH1, and ACTN2 using the ICC assay after treatments with peptide **1**, vesicles, and sheets, respectively (excitation wavelength at λ_{ex} = 488 nm and emission wavelength at λ_{em} = 525 nm). (h) Representative western blotting results for the protein expression of ITG $\alpha 2\beta 1$, MYOG, MYH1, and ACTN2 after the treatment of peptide **1**, vesicles, and sheets. Control indicates that the material was not treated. Means ± SEM ($n \geq 3$). *p < 0.032, **p < 0.0021, and ***p < 0.0002.

ratio of peptide **2**. Therefore, higher DGEA peptide density in the 2D materials is important to maximize the cellular proliferation effect.

We performed a wound healing assay to evaluate the effect of the peptide assemblies and peptide **1** on the migratory abilities of C2C12 cells, and the treatment of peptide **1** did not result in a remarkable change in the migration rate (compared with non-

https://doi.org/10.1021/jacs.2c10938
J. Am. Chem. Soc. 2023, 145, 1793−1802

treated plates; control) (Figure 5b). However, the migration rates of vesicles and sheets were increased by approximately 29 and 36%, respectively, indicating that the self-assembled peptide materials could substantially stimulate myoblast proliferation. To further investigate whether the results of the enhanced proliferation rate were stimulated *via* the target proteins or not, we measured the expression of integrin $\alpha2\beta1$ (ITG $\alpha2\beta1$) by western blotting and immunocytochemistry (ICC) because the peptide sequence DGEA is reported to bind with the integrin $\alpha2\beta1$ receptor. The expression of integrin $\alpha2\beta1$ was higher in the sample treated in sheets than in the sample treated in monomeric peptides and vesicles (Figure 5c). Indeed, the proliferation marker protein Ki-67[22] as a nuclear protein associated with the transcription factor exhibited a higher expression level due to integrin $\alpha2\beta1$ upregulation of the cells grown on the 2D peptide assembly (Figures 5d and S25).

Additionally, the peptide assemblies were assessed to investigate the response in the differentiation of C2C12 cells, as the ligand binding to integrin $\alpha2\beta1$ receptors can stimulate the remodeling of myoblast cells to form mature myotubes in parallel with the increased expression of muscle-specific proteins. A 15% increase in the fusion indices was observed in the sample with the sheets, indicative of enhanced muscle differentiations (Figure 5e,f). Protein expression levels of integrin $\alpha2\beta1$ and differentiation marker proteins such as myogenin (MYOG),[23] myosin heavy chain1 (MYH1),[24] and actinin2 (ACTN2)[25] were increased significantly in cells grown on 2D peptide materials (Figures 5g,h and S26). Taking all the data together, the 2D assembly of the DGEA peptide could play the role of an activator of integrin $\alpha2\beta1$ and promote muscle cell proliferation and differentiation during myogenesis. These results imply that peptide-based supramolecular 2D flat structures with relatively larger sizes and better structural stabilities *via* arene−perfluoroarene interaction can continuously stimulate cell surface receptors in the extracellular environment without significant cellular internalization. Eventually, the 2D peptide assembly effectively transmits signals to cells *via* integrin $\alpha2\beta1$, and the resulting intracellular signaling regulates biological activity through the stimulation of transcription factors in the nucleus, such as Ki-67 or MYOG.

CONCLUSIONS

We demonstrated the formation of supramolecular vesicles and 2D sheets by self-assembly of the pyrene-grafted amphiphilic peptide **2** in an aqueous solution. The 2D assembly was formed *via* the arene−perfluoroarene interaction between the pyrene segment and OFN, showing enhanced structural stability and a large size due to the compact face-centered stacking by strong aromatic interaction *via* electrostatic attraction. The bioactive DGEA peptide segment on 2D structures was exposed to the aqueous environment for interaction with the target protein. DGEA-coated 2D materials with structural stability, a flat structure, and a larger size could increase the expression of the integrin $\alpha2\beta1$ receptor on the membrane surface of C2C12 cells without significant internalization into the intracellular environment. As a result, 2D peptide assembly could enhance the proliferation and differentiation of myoblasts more than those in the monomeric DGEA peptide and vesicles with the same peptide fragments *via* continuous interactions with the integrin $\alpha2\beta1$ receptor. The 2D assembly based on bioactive peptides can provide many insights for the development of next-generation biomaterials by overcoming conventional peptide limitations such as shorter *in vivo* retention time and rapid proteolytic degradations.

MATERIALS AND METHODS

General Methods. All starting materials obtained from commercial suppliers (TCI, Anaspec, Novabiochem, TCI, *etc.*) were used without further purification. Peptides **1** and **2** were prepared according to the procedures described previously.[26] Dichloromethane (DCM) was dried by distillation from CaH_2. Distilled water (DW) was prepared by ion exchange and filtration. Other solvents and organic reagents were purchased from commercial vendors and used without further purification unless otherwise mentioned. Mass spectrometry was performed on an Expression CMS (Advion) electrospray ionization (ESI) mass spectrometer and a SYNAPT G2 high-definition mass spectrometer (HDMS) system (Waters). HPLC analysis was performed on a YL9100 HPLC system equipped with a YMC-Pack Pro C18 reverse phase column (C18, 250 × 4.6 mm I.D.) for analysis and YMC-Triart C18 (250 × 10.0 mm I.D. S-5 μm) for separation. UV−vis spectra were measured using an Agilent 8453E UV−visible spectroscope, and fluorescence spectra were obtained from a Hitachi F-7000 fluorescence spectrophotometer. Circular dichroism (CD) spectra were measured using a JASCO J-1100 spectropolarimeter. CD spectra were recorded from 600 to 180 nm using a 1 mm path length cell. Scans were repeated three times and averaged. Samples have been kept at room temperature for 24 h before the measurement. Sizes of the vesicle and the 2D sheets were characterized by DLS at a fixed angle of θ = 90° using a BI-200SM (Brookhaven Instruments Corporation, USA) with a laser beam wavelength of 636 nm. ^{1}H NMR spectra were obtained on a 400 MHz FT-NMR spectrometer using JNM-ECZ400S/L1. X-ray scattering measurements were performed in the transmission mode with synchrotron radiation at the 3C X-ray beamline at the Pohang Accelerator Laboratory.

TEM Experiments. To investigate the self-assembled structures in aqueous solution, a drop of each sample solution was placed on a carbon-coated copper grid [Carbon Type B (15−25 nm) on 200 mesh, with Formvar; Ted Pella, Inc.], and the solution was allowed to evaporate under ambient conditions. These samples were stained by depositing a drop of uranyl acetate aqueous solution (0.4 wt %) on the surface of the sample-loaded grid. The dried specimen was observed using a Hitachi H-7100 operated at 100 kV. The data were analyzed using ImageJ.

AFM Experiments. The sample films on the mica surface were prepared from the evaporation of 0.01 wt % peptide **2** with OFN solution in DW. AFM measurements were subsequently performed using an NX-10 (Park systems) to determine the thicknesses of monolayers. The data were analyzed using XEI analysis software.

^{1}H NMR Experiments. ^{1}H NMR (400 MHz) spectra were recorded in a solution of peptide **2** and peptide **2** with OFN in D_2O-containing 1 mM phosphate buffer at a pH of 7.4 with a concentration of 687 μM.

Molecular Simulations. All the computations were performed using the Gaussian 09 program. Methoxypyrene, OFN, HFB, and fluoranil were calculated by the DFT B3LYP/6-31G(d) method. Mulliken atomic charges, dipole moments (DMs), and molecular orbital energy levels of the methoxypyrene complex with OFN, HFB, and fluoranil in the gas state were simulated using the DFT M06-2X/6-31G(d) method.

XRD Experiments. To prepare the powder sample, each molecule in the phosphate buffer at a pH of 7.4 was transferred to the X-ray holder and then measured after drying.

Cell Cultures. Murine myoblast C2C12 cells (Korean Cell Line Bank, Seoul, Korea) were cultured in DMEM (Dulbecco's modified Eagle's medium; HyClone, Logan, UT, USA) supplemented with 10% (for cell proliferation) or 2% (for cell differentiation) FBS (fetal bovine serum, Equitech-Bio) and 1% P/S (penicillin/streptomycin, Hyclone Laboratories, Logan, UT, USA). At 90−95% cell confluency, the cell culture medium was changed with a differentiation medium, and the medium was replaced every 1−2 days.

MTT Assay. For cell toxicity and proliferation analyses, C2C12 cells were cultured in proliferation media (10% FBS) and incubated for 2

https://doi.org/10.1021/jacs.2c10938
J. Am. Chem. Soc. 2023, 145, 1793−1802

days. Cells were then washed with phosphate-buffered saline (PBS) and incubated with thiazolyl blue tetrazolium bromide (0.5 mg/mL; Sigma-Aldrich, St. Louis, MO, USA) for 1 h. The generated formazan crystals were dissolved in dimethyl sulfoxide (DMSO) (Sigma-Aldrich), and the absorbance was measured at 570 nm (Epoch, Biotec, USA).

Wound Healing Assay. For the *in vitro* scratch assay, cells (5×10^4 cells per well) were plated in a 24-well plate using CytoSelect Wound Healing Inserts (Cell Biolabs, Inc.) and incubated at 37 °C until a monolayer wasformed. Thereafter, inserts were removed from the plate well, and the cells were thoroughly washed with PBS and incubated with fresh medium. Wound closure was monitored by collecting the images at 0 and 48 h intervals, and digital images were captured by using an inverted microscope (Olympus). The images were obtained at the same position before and after incubation. The experiment was repeated three times. The level of wound healing was calculated relatively by the ratio of the closure area to the area of the initial wound (0 h) as follows

$$R_n = (A_0 - A_n)/A_0 \times 100\%$$

where R_n represents the percentage of wound closure, A_n represents the residual area of the wound at the metering point (n hours), and A_0 represents the area of the initial wound (0 h). Area calculation was performed using ImageJ software (USA).

Western Blot. Cells were lysed with the radioimmunoprecipitation assay (RIPA) buffer containing the protease inhibitor cocktail (GenDEPOT), and total proteins were quantified using the Bradford assay. Total protein extracts (50 μg) were run on sodium dodecyl sulfate−polyacrylamide gel electrophoresis (SDS-PAGE) (6−10%) and transferred onto polyvinylidene fluoride (PVDF) membranes (GenDEPOT) using the Bio-Rad mini protein transfer system (Bio-Rad, Hercules, CA, USA). The protein-transferred membrane was blocked with 5% skim milk/Tris-buffered saline (TBS) containing Tween 20 for 1 h at room temperature. Blocked membranes were then incubated with the primary antibodies diluted with TBS (the ratio of the volume of the antibodies to the total volume of TBS as follows: Ki-67, 1:500; ITG $\alpha 2\beta 1$, 1:500; β-actin, 1:1000; MYOG, 1:500; MYH1, 1:500; and ACTN2, 1:500) overnight at 4 °C. After washing, the blots were incubated with horseradish peroxidase-conjugated secondary antibodies (goat anti-mouse or anti-rabbit; 1:1000, GenDePOT) at room temperature for 2 h and developed using the West-Q Pico ECL Solution (GenDEPOT).

Immunocytochemistry. Cells were fixed with 4% formaldehyde (Sigma-Aldrich) for 15 min, permeabilized with 0.2% Triton X-100 (Sigma-Aldrich), and subsequently incubated overnight with the primary antibodies with PBS (the ratio of the volume of the antibodies to the total volume of PBS as follows: Ki-67, 1:100; ITG $\alpha 2\beta 1$, 1:100; MYOG, 1:100; MYH1, 1:100; and ACTN2, 1:100) at 4 °C in a humid environment. Secondary antibodies (1:100; Alexa Fluor 594 or 488 goat anti-rabbit and goat anti-mouse; Thermo Fisher Scientific) were applied for 1 h at room temperature, and the fluorescence images were obtained using a fluorescence microscope equipped with an inverted microscope (Olympus, IX73, Japan).

Fusion Index. The fusion index was analyzed as described previously.[27] In brief, cells were fixed with methanol/PBS (1:1), nuclei were stained with 0.04% Giemsa G250 (Sigma-Aldrich) for 30 min and then washed with PBS, and images were taken randomly at three different spots. Additionally, the number of nuclei in myotubes and the total number of nuclei in cells were counted in each field.

Cell Uptake Analysis. For the cell uptake efficiency test, cells (2×10^5 cells per well) were plated in 100 mm dish plates and treated to peptide **2** (vesicle) and peptide **2** with OFN (sheet) at 5 μM concentration. To indicate control, empty plates were treated with a 5 μM concentration of peptide **2** and incubated for 4 days. Thereafter, cell culture media were collected from the plates, and the remaining peptide **2** was retrieved using an additional PBS buffer. The collected samples were dried by nitrogen evaporation, and the amount with the same volume used the solvable solvent MeOH/DW (8:2, v/v). Each sample was injected at 100 μL for HPLC analysis. Peptide **2** was analyzed by solvent water/acetonitrile with 0.1% trifluoroacetic acid using the C18 column. The HPLC analysis was performed in the gradient mobile phase (Table 1).

Peptide Degradations. Digestion of peptide bonds on peptide **1**, vesicle, and sheet materials were measured by protease activity from the bovine pancreas. Each sample of 300 μM concentration was prepared in 2.0 mM calcium acetate buffer and incubated at 30 °C for 5 min. The enzyme solution of 50 mg/mL from bovine pancreas containing 2.0 mM calcium acetate buffer was mixed and then incubated for 30 °C at 15 min. The TCA mixture containing 0.11 M trichloroacetic acid, 0.22 M sodium acetate, and 0.33 M acetic acid was added to each sample for reaction termination and incubated for a further 20 min at 30 °C. Degradations of samples *via* protease were analyzed *via* HPLC (water/acetonitrile with 0.1% trifluoroacetic acid).

Pyrene Degradations. The chemical stability of the pyrene segment was measured through degradations by cytochrome P450 1A2 (CYP1A2). Each supramolecular material of 500 μM concentration was prepared in a 100 mM potassium phosphate buffer at a pH of 7.4 containing 5.0 mM glucose-6-phosphate (G6P, TCI) and 2.0 mM nicotinamide adenine dinucleotide phosphate ($NADP^+$, TCI). 20 mg/mL *CypExpress* (Sigma-Aldrich) was added to the stirred suspension of the sample solutions. The mixtures were kept at 37 °C during the different incubation times. Quenching of the enzyme reaction was performed with 1.0 mL of acetonitrile. HPLC analysis measured the degradation of samples *via* cytochrome P450 (water/acetonitrile with 0.1% trifluoroacetic acid).

Statistical Analysis. Normalized fluorescence intensity means were compared using Tukey's Studentized Range to identify significant differences in fluorescence intensity (protein expression). Bonferroni's multiple comparisons test was used for the comparison of two different materials (cell uptake efficiency). Fluorescence intensity means of cell retention time about two different materials were obtained by Tukey's multiple comparisons test. Nominal p-values of less than 0.05 are considered statistically significant (Prism-GraphPad, San Diego, CA, USA).

■ ASSOCIATED CONTENT

Supporting Information

The Supporting Information is available free of charge at https://pubs.acs.org/doi/10.1021/jacs.2c10938.

Synthetic methods; ^{1}H NMR, mass spectra; HPLC data of compounds; UV spectra; fluorescence spectra; 2D NOE NMR spectra; MD simulations; DFT calculations; XRD data; zeta potential measurements; additional TEM, FOM, and AFM images; and MTT assay results of the samples (PDF).

■ AUTHOR INFORMATION

Corresponding Author

Yongju Kim − *KU-KIST Graduate School of Converging Science and Technology, Korea University, Seoul 02841, Republic of Korea; Department of Integrative Energy Engineering, Korea University, Seoul 02841, Republic of Korea;* orcid.org/0000-0002-5862-5228; Email: yongjukim@korea.ac.kr

Authors

Taeyeon Kim − *KU-KIST Graduate School of Converging Science and Technology, Korea University, Seoul 02841, Republic of Korea*

Jinwoo Hong − *KU-KIST Graduate School of Converging Science and Technology, Korea University, Seoul 02841, Republic of Korea*

Jehan Kim − *Pohang Accelerator Laboratory, POSTECH, Pohang 37673 Gyeongbuk, Republic of Korea*

Jinhan Cho − *Department of Chemical and Biological Engineering, Korea University, Seoul 02841, Republic of Korea;* orcid.org/0000-0002-7097-5968

https://doi.org/10.1021/jacs.2c10938
J. Am. Chem. Soc. 2023, 145, 1793−1802

Complete contact information is available at:
https://pubs.acs.org/10.1021/jacs.2c10938

Notes

The authors declare no competing financial interest.

■ ACKNOWLEDGMENTS

This work was supported by the National Research Foundation of Korea grant funded by the Korean government (NRF-2019R1C1C1008526, NRF-2019R1A4A1027627, NRF-2022R1F1A1075138, and NRF-2022R1A4A1031687), a Korea University grant, and the KU-KIST School Project.

■ ABBREVIATIONS

OFN	octafluoronaphthalene
DLS	dynamic light scattering
TEM	transmission electron microscopy
HFB	hexafluorobenzene
CD	circular dichroism
AFM	atomic force microscopy
XRD	X-ray diffraction
1H NMR	proton nuclear magnetic resonance
HPLC	high-performance liquid chromatography
ICC	immunocytochemistry
MYOG	myogenin
MYH1	myosin heavy chain1
ACTN2	actinin2

■ REFERENCES

(1) Savyasachi, A. J.; Kotova, O.; Shanmugaraju, S.; Bradberry, S. J.; Ó'Máille, G. M.; Gunnlaugsson, T. Supramolecular chemistry: a toolkit for soft functional materials and organic particles. *Chem* **2017**, *3*, 764−811.

(2) (a) Kim, H.-J.; Kim, T.; Lee, M. Responsive nanostructures from aqueous assembly of rigid−flexible block molecules. *Acc. Chem. Res.* **2011**, *44*, 72−82. (b) Kim, Y.; Shin, S.; Kim, T.; Lee, D.; Seok, C.; Lee, M. Switchable nanoporous sheets by the aqueous self-assembly of aromatic macrobicycles. *Angew. Chem., Int. Ed.* **2013**, *52*, 6426−6429.

(3) (a) Webber, M. J.; Langer, R. Drug delivery by supramolecular design. *Chem. Soc. Rev.* **2017**, *46*, 6600−6620. (b) Jin, X.; Zhu, L.; Xue, B.; Zhu, X.; Yan, D. Supramolecular nanoscale drug-delivery system with ordered structure. *Natl. Sci. Rev.* **2019**, *6*, 1128−1137.

(4) Geng, W.-C.; Ye, Z.; Zheng, Z.; Gao, J.; Li, J.-J.; Shah, M. R.; Xiao, L.; Guo, D.-S. Supramolecular bioimaging through signal amplification by combining indicator displacement assay with förster resonance energy transfer. *Angew. Chem., Int. Ed.* **2021**, *60*, 19614−19619.

(5) Voskuhl, J.; Sankaran, S.; Jonkheijm, P. Optical control over bioactive ligands at supramolecular surfaces. *Chem. Commun.* **2014**, *50*, 15144−15147.

(6) (a) Hersel, U.; Dahmen, C.; Kessler, H. RGD modified polymers: biomaterials for stimulated cell adhesion and beyond. *Biomaterials* **2003**, *24*, 4385−4415. (b) Auernheimer, J.; Dahmen, C.; Hersel, U.; Bausch, A.; Kessler, H. Photoswitched cell adhesion on surfaces with RGD peptides. *J. Am. Chem. Soc.* **2005**, *127*, 16107−16110. (c) Mou, X.; Zhang, H.; Qiu, H.; Zhang, W.; Wang, Y.; Xiong, K.; Huang, N.; Santos, H. A.; Yang, Z. Mussel-inspired and bioclickable peptide engineered surface to combat thrombosis and infection. *Research* **2022**, *2022*, 9780879.

(7) Luo, Z.; Zhang, S.; Pan, J.; Shi, R.; Liu, H.; Lyu, Y.; Han, X.; Li, Y.; Yang, Y.; Xu, Z.; Sui, Y.; Luo, E.; Zhang, Y.; Wei, S. Time-responsive osteogenic niche of stem cells: A sequentially triggered, dual-peptide loaded, alginate hybrid system for promoting cell activity and osteo-differentiation. *Biomaterials* **2018**, *163*, 25−42.

(8) (a) Lu, J.; Shen, X.; Sun, X.; Yin, H.; Yang, S.; Lu, C.; Wang, Y.; Liu, Y.; Huang, Y.; Yang, Z.; Dong, X.; Wang, C.; Guo, Q.; Zhao, L.; Sun, X.; Lu, S.; Mikos, A. G.; Peng, J.; Wang, X. I. Increased recruitment of endogenous stem cells and chondrogenic differentiation by a composite scaffold containing bone marrow homing peptide for cartilage regeneration. *Theranostics* **2018**, *8*, 5039−5058. (b) Hivare, P.; Gangrade, A.; Swarup, G.; Bhavsar, K.; Singh, A.; Gupta, R.; Thareja, P.; Gupta, S.; Bhatia, D. Peptide functionalized DNA hydrogel enhances neuroblastoma cell growth and differentiation. *Nanoscale* **2022**, *14*, 8611−8620.

(9) Saric, T.; Graef, C. I.; Goldberg, A. L. Pathway for degradation of peptides generated by proteasomes: a key role for thimet oligopeptidase and other metallopeptidases. *J. Biol. Chem.* **2004**, *279*, 46723−46732.

(10) Arslan, E.; Garip, I. C.; Gulseren, G.; Tekinay, A. B.; Guler, M. O. Bioactive supramolecular peptide nanofibers for regenerative medicine. *Adv. Healthcare Mater.* **2014**, *3*, 1357−1376.

(11) (a) Sato, K.; Hendricks, M. P.; Palmer, L. C.; Stupp, S. I. Peptide supramolecular materials for therapeutics. *Chem. Soc. Rev.* **2018**, *47*, 7539−7551. (b) Shang, Y.; Zhi, D.; Feng, G.; Wang, Z.; Mao, D.; Guo, S.; Liu, R.; Liu, L.; Zhang, S.; Sun, S.; Wang, K.; Kong, D.; Gao, J.; Yang, Z. Supramolecular nanofibers with superior bioactivity to insulin-like growth factor-I. *Nano Lett.* **2019**, *19*, 1560−1569.

(12) (a) Diaferia, C.; Gianolio, E.; Accardo, A. Peptide-based building blocks as structural elements for supramolecular Gd-containing MRI contrast agents. *J. Pept. Sci.* **2019**, *25*, No. e3157. (b) Chang, R.; Zou, Q.; Xing, R.; Yan, X. Peptide-based supramolecular nanodrugs as a new generation of therapeutic toolboxes against cancer. *Adv. Ther.* **2019**, *2*, 1900048. (c) Klass, S. H.; Smith, M. J.; Fiala, T. A.; Lee, J. P.; Omole, A. O.; Han, B.-G.; Downing, K. H.; Kumar, S.; Francis, M. B. Self-assembling micelles based on an intrinsically disordered protein domain. *J. Am. Chem. Soc.* **2019**, *141*, 4291−4299.

(13) (a) Wang, H.; Yan, Y.-Q.; Yi, Y.; Wei, Z.-Y.; Chen, H.; Xu, J.-F.; Wang, H.; Zhao, Y.; Zhang, X. Supramolecular peptide therapeutics: host-guest interaction-assisted systemic delivery of anticancer peptides. *CCS Chem.* **2020**, *2*, 739−748. (b) Fatouros, D. G.; Lamprou, D. A.; Urquhart, A. J.; Yannopoulos, S. N.; Vizirianakis, I. S.; Zhang, S.; Koutsopoulos, S. Lipid-like self-assembling peptide nanovesicles for drug delivery. *ACS Appl. Mater. Interfaces* **2014**, *6*, 8184−8189.

(14) (a) Haffner, A.; Hatz, A.-K.; Zeman, O. E. O.; Hoch, C.; Lotsch, B. V.; Johrendt, D. Polymorphism and Fast Potassium-Ion Conduction in the T5 Supertetrahedral Phosphidosilicate KSi2P3. *Angew. Chem., Int. Ed. Engl.* **2021**, *60*, 13641−13646. (b) Insua, I.; Montenegro, J. 1D to 2D Self Assembly of Cyclic Peptides. *J. Am. Chem. Soc.* **2020**, *142*, 300−307.

(15) (a) Kim, T.; Park, J. Y.; Hwang, J.; Seo, G.; Kim, Y. Supramolecular two-dimensional systems and their biological applications. *Adv. Mater.* **2020**, *32*, No. e2002405. (b) Shen, B.; Kim, Y.; Lee, M. Supramolecular chiral 2D materials and emerging functions. *Adv. Mater.* **2020**, *32*, No. e1905669.

(16) (a) Huang, C.-C.; Kang, M.; Shirazi, S.; Lu, Y.; Cooper, L. F.; Gajendrareddy, P.; Ravindran, S. 3D encapsulation and tethering of functionally engineered extracellular vesicles to hydrogels. *Acta Biomater.* **2021**, *126*, 199−210. (b) Hu, H.; Masarapu, H.; Gu, Y.; Zhang, Y.; Yu, X.; Steinmetz, N. F. Physalis mottle virus-like nanoparticles for targeted cancer imaging. *ACS Appl. Mater. Interfaces* **2019**, *11*, 18213−18223. (c) Liu, S.; Ngo, U.; Tang, X. Z.; Ren, X.; Qiu, W.; Huang, X.; DeGrado, W.; Allen, C. D.; Jo, H.; Sheppard, D.; Sundaram, A. B. Integrin $\alpha 2\beta 1$ regulates collagen I tethering to modulate hyperresponsiveness in reactive airway disease models. *J. Clin. Invest.* **2021**, *131*, No. e138140.

(17) (a) Jallerat, Q.; Feinberg, A. W. Extracellular matrix structure and composition in the early four-chambered embryonic heart. *Cells* **2020**, *9*, 285. (b) Sun, B. The mechanics of fibrillar collagen extracellular matrix. *Cell Rep. Phys. Sci.* **2021**, *2*, 100515. (c) Buehler, M. J. Nature designs tough collagen: explaining the nanostructure of collagen fibrils. *Proc. Natl. Acad. Sci. U.S.A.* **2006**, *103*, 12285−12290.

(18) Lee, G. Y.; Hu, E.; Rheingold, A. L.; Houk, K. N.; Sletten, E. M. Arene-perfluoroarene interactions in solution. *J. Org. Chem.* **2021**, *86*, 8425−8436.

(19) Shetty, A. S.; Zhang, J.; Moore, J. S. Aromatic π-Stacking in Solution as Revealed through the Aggregation of Phenylacetylene Macrocycles. *J. Am. Chem. Soc.* **1996**, *118*, 1019−1027.

(20) (a) Furge, L. L.; Guengerich, F. P. Cytochrome P450 enzymes in drug metabolism and chemical toxicology: An introduction. *Biochem. Mol. Biol. Educ.* **2006**, *34*, 66−74. (b) Sesardic, D.; Boobis, A. R.; Murray, B. P.; Murray, S.; Segura, J.; de la Torre, R.; Davies, D. S. Furafylline is a potent and selective inhibitor of cytochrome P450IA2 in man. *Br. J. Clin. Pharmacol.* **1990**, *29*, 651−663.
(21) (a) Jain, M.; Chauhan, A. K. Role of integrins in modulating smooth muscle cell plasticity and vascular remodeling: from expression to therapeutic implications. *Cells* **2022**, *11*, 646. (b) Sivaraman, K.; Shanthi, C. Matrikines for therapeutic and biomedical applications. *Life Sci.* **2018**, *214*, 22−33.
(22) (a) Sales Gil, R.; Vagnarelli, P. Ki-67: More Hidden behind a 'Classic Proliferation Marker'. *Trends Biochem. Sci.* **2018**, *43*, 747−748. (b) Sun, X.; Kaufman, P. D. Ki-67: more than a proliferation marker. *Chromosoma* **2018**, *127*, 175−186.
(23) (a) Ganassi, M.; Badodi, S.; Wanders, K.; Zammit, P. S.; Hughes, S. M. Myogenin is an essential regulator of adult myofibre growth and muscle stem cell homeostasis. *Elife* **2020**, *9*, No. e60445. (b) Ganassi, M.; Badodi, S.; Ortuste Quiroga, H. P.; Zammit, P. S.; Hinits, Y.; Hughes, S. M. Myogenin promotes myocyte fusion to balance fibre number and size. *Nat. Commun.* **2018**, *9*, 4232.
(24) (a) Stern-Straeter, J.; Bonaterra, G. A.; Kassner, S. S.; Zügel, S.; Hörmann, K.; Kinscherf, U. R.; Goessler, J. Characterization of human myoblast differentiation for tissue-engineering purposes by quantitative gene expression analysis. *J. Regen. Med. Tissue Eng.* **2011**, *5*, e197−e206. (b) Agarwal, M.; Sharma, A.; Kumar, P.; Kumar, A.; Bharadwaj, A.; Saini, M.; Kardon, G.; Mathew, S. J. Myosin heavy chain-embryonic regulates skeletal muscle differentiation during mammalian development. *Development* **2020**, *147*, dev184507.
(25) Arvanitis, M.; Tampakakis, E.; Zhang, Y.; Wang, W.; Auton, A.; Agee, D.; Aslibekyan, S.; Bell, A.; Bryc, N.; Clark, N. C.; Elson, B.; Fletez-Brant, W. S.; Fontanillas, A.; Furlotte, N. A.; Gandhi, P. M.; Heilbron, K.; Hicks, B.; Hinds, D. A.; Huber, K. E.; Jewett, E. M.; Jiang, Y.; Kleinman, A.; Lin, K.-H.; Litterman, N. K.; McCreight, J. C.; McIntyre, M. H.; McManus, K. F.; Mountain, J. L.; Mozaffari, S. V.; Nandakumar, P.; Noblin, E. S.; Northover, C. A. M.; O'Connell, J.; Pitts, S. J.; Poznik, G. D.; Sathirapongsasuti, J. F.; Shastri, A. J.; Shelton, J. F.; Shringarpure, S.; Tian, C.; Tung, J. Y.; Tunney, R. J.; Vacic, V.; Wang, X.; Zare, A. S.; Dutta, D.; Glavaris, S.; Keramati, A.; Chatterjee, N.; Chi, N. C.; Ren, B.; Post, W. S.; Battle, A. Genome-wide association and multi-omic analyses reveal ACTN2 as a gene linked to heart failure. *Nat. Commun.* **2020**, *11*, 1122.
(26) Chen, X.; Wang, H.; Wang, Y.; Kim, M.; Lee, M. α-Helical peptide vesicles with chiral membranes as enantioselective nanoreactors. *Chem. Commun.* **2017**, *53*, 10958−10961.
(27) Lee, E. J.; Pokharel, S.; Jan, A. T.; Huh, S.; Galope, R.; Lim, J. H.; Lee, D. M.; Choi, S. W.; Nahm, S.-S.; Kim, Y.-W.; Park, S.-Y.; Choi, I. Transthyretin: A Transporter Protein Essential for Proliferation of Myoblast in the Myogenic Program. *Int. J. Mol. Sci.* **2017**, *18*, 115.

https://doi.org/10.1021/jacs.2c10938
J. Am. Chem. Soc. 2023, 145, 1793−1802